Preparation and Mechanical Properties of Mullites and Mullite–Zirconia Composites

Yoshitaka KUBOTA

Hiroyoshi TAKAGI*

High–purity stoichiometric mullite and mullite–zirconia composite powders were prepared by calcination of the products precipitated from two different systems of an aqueous solution of $Al(NO_3)_3$/colloidal SiO_2 and $Al(NO_3)_3$/$ZrOCl_2$/colloidal SiO_2. The precipitated products transformed into mullite via an exothermic reaction at 1250°C. Tetragonal ZrO_2 particles were formed above 800°C in the composite powders. In the range of 70 to 78 wt% Al_2O_3, the pure mullite containing 70 and 72 wt% Al_2O_3 showed the highest fracture strength above 1000°C because of a glassy phase present along the grain boundaries and the acicular grain shape. On the other hand, fracture strength of mullite–ZrO_2 composites increased with increasing ZrO_2 volume fraction. Dispersion of ZrO_2 particles enhanced the strength of the matrix in a temperature range from room temperature to 900°C. The toughening mechanism seems to be a combination of transformation toughening and other mechanisms such as microcracking and/or crack deflection.

1. Introduction

Mullite is one of the basic constituents of traditional refractories. It is attractive because of its high temperature mechanical stability, creep resistance, chemical resistance, low thermal expansion and dielectric constant. However, since mullite is difficult to be consolidated into fully dense, high–purity stoichiometric bodies. To overcome these difficulties, some investigators have attempted to prepare high–purity and active mullite powders, using co–precipitation[1], organo–metallic[2] and freeze–drying[3] procedures.

In the present study, fine, high–purity powders were prepared by calcination of the products precipitated from mixed aqueous solutions of aluminium nitrate 9–hydrate and colloidal silica. After an appropriate consolidation process, the mechanical properties of the ceramics, such as fracture strength, fracture toughness and slow crack growth behavior, were studied at room temperature to 1400°C.

Mullite–zirconia composites was also prepared using a similar method. This is attempted in view of the previous reports in the literature[4,5,6] that dispersed ZrO_2 particles significantly improve the fracture property of the mullite composites.

2. Experimental Procedures

2—1. Powder preparation

A co–precipitation method using an aqueous solution of (a) $Al(NO_3)_3$ and colloidal SiO_2 and (b) $Al(NO_3)_3$, $ZrOCl_2$ and colloidal SiO_2 was employed. A typical procedure was conducted as follows:

*Government Industrial Research Institute, Nagoya, JAPAN

an aqueous solution of NH_4OH (14 wt%NH_3) was quickly added to an aqueous solution of $Al(NO_3)_3$ containing colloidal SiO_2 to form a gel under the condition of continuous stirring, with the pH of the solution adjusted to fall into between 6.5 and 7.5 so that it gives the minimum solubility of $Al(OH)_3$. The mixed hydroxide prepared was then filtered on a Büchner funnel, and the precipitate was washed using distilled water. The precipitate was dried on a shallow tray at 80°C overnight, followed by calcining in an Al_2O_3 crucible at 1300°C for 1 h. The calcined material was wet ball–milled for 72 h in an alumina jar using alumina balls and ethanol. After ball–milling the slurry was dried to produce fine mullite powders.

Powder characterization by X–ray diffraction and DTA was made, and the particle morphology of the powders was examined by TEM.

2—2. Consolidation and Testing·

About 10 g of prepared powders were cold die–pressed into rectangular blocks, followed by cold isostatic pressing at a total pressure of 250MPa. The compacts were consolidated by pressureless sintering in an electric furnace in air.

Sintered bodies were machined into test bars (3.5 cm by 0.4 cm by 0.3 cm). All faces were ground in the lengthwise direction using 400 grit diamond wheels and the edges were chamfered to prevent notch effects. The surface to be submitted to tension in bending for the measurements of fracture toughness was carefully ground and wet polished to 3 μm diamond finish.

The fracture strength of the materials was measured by a three–point bending method in a testing machine operated at a constant cross–head speed of 0.5 mm/min, where the span was fixed as 3.0 cm. The controlled surface flaw method[7] using Knoop Diamond microhardness indentation was also used to measure the fracture toughness. A 9.8 N indentation load was used to produce a nearly semicircular microcrack having a radius of $\cong 130$ μm. The testing for fracture strength was done at room temperature to 1400°C in air. Prior to loading, specimens were held at the test temperature for about 15 min in order to achieve thermal equilibrium. Fracture surfaces were examined by SEM. Tetragonal ZrO_2 fraction was measured on an as–sintered surface using integrated X–ray diffraction intensities[8]. The micro–indentation method[9] was also used to measure the fracture toughness.

3. Results and Discussion

3—1. Powders preparation

The DTA heating curve obtained for the co–precipitated powder with $Al_2O_3/SiO_2=72/28$ (in weight) is shown in Fig. 1. A broad endotherm at 200°C due to the loss of water and two exothermic peaks at 260°C and 1250°C can be seen. The first exotherm at 260°C is attributed to decomposition of nitrate (NH_4NO_3). To investigate the origin of the second exotherm, X–ray powder diffraction patterns were obtained for the precipitates submitted to the DTA near 1250°C. The results are shown in
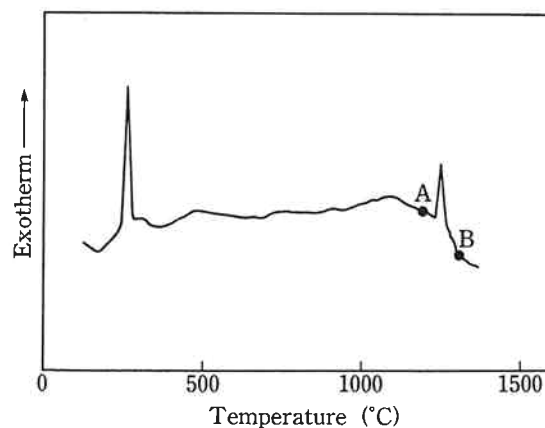

Fig. 1. The DTA heating curve obtained for the co–precipitated powder with Al_2O_3/SiO_2 =72/28 (in weight).

Fig. 2. The X–ray chart obtained at point A in the DTA curve shows that the precipitate is a mixture of a γ–Al_2O_3–like phase and amorphous SiO_2 (or fine crystalline of cristobalite[10]), and the X–ray chart at point B shows the presence of mullite phase with no evidence of crystalline Al_2O_3 and SiO_2. These X–ray data suggests that the second exotherm at 1250°C is due to the formation of mullite. Previously, Hoffman et al.[10] reported that gels prepared by gelling colloidal SiO_2 and $Al(NO_3)_3$ showed no trace of the exotherm of mullite formation. Instead, there was an apparently continuous reaction over a range of several hundred degrees. The different behaviour between these two studies are likely due to the difference in the degree of mixing between $Al(OH)_3$ and SiO_2 in the gel. Fig. 3. is a TEM photograph of the precipitate heated at 1000°C for 1 h. It may be recognized that $Al(OH)_3$ and SiO_2 particles in the co-precipitated powder are well mixed and their average grain sizes are in the range of 10 to 40 nm. Metakaolinite[11] and a gell derived from metal alkoxides[1], in which Al_2O_3 and SiO_2 were mixed on the unit–cell scale, have been reported to indicate two exotherms at 960°C and 1250°C in the DTA curve. The exotherm at 960°C was attributed to both mullite formation and Al–Si spinel formation, while the exotherm at 1250°C was attributed to the transformation of the spinel to mullite. On the other hand, Kanzaki et al.[12] found that amorphous mullite transformed to mullite with an exotherm at 960°C. They reported that the amorphous mullite was prepared by spray pyrolysis of a mixed solution of $Al(NO_3)_3$ and ethylsilicate, where Al and Si ions were considered to be mixed on the atomic scale. These results all suggest that the degree of mixing of Al and Si ions in the co–precipitated powders significantly influence the mullitization temperature.
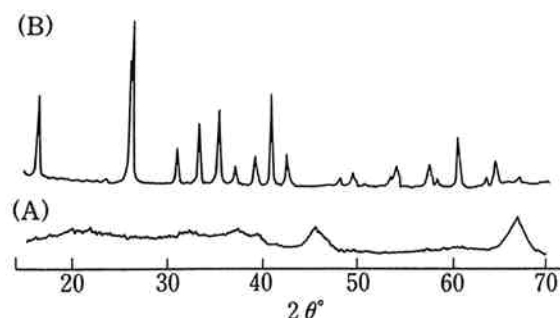

Fig. 2. X–ray powder diffraction patterns obtained for the precipitates which were submitted to the DTA experiments.

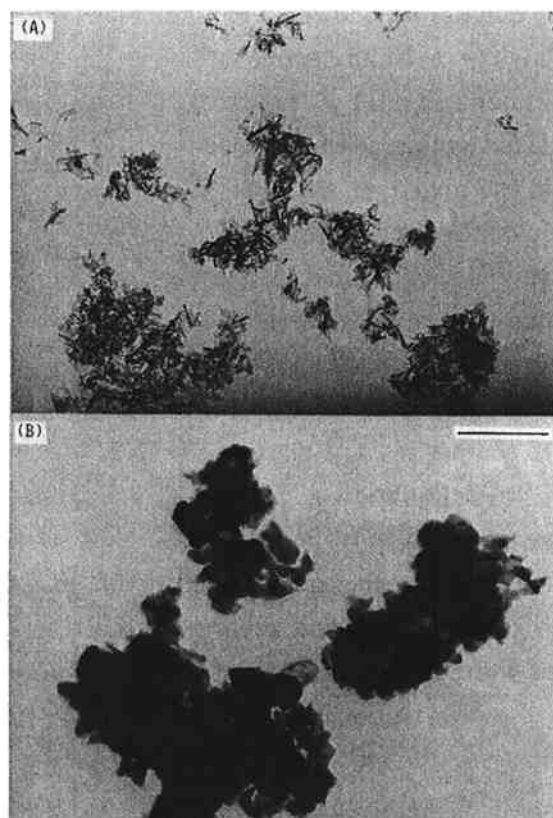Fig. 3. TEM photogsaphs of the precipitates heated
(A) at 1000°C for 1 h,
(B) at 1300°C for 1 h, (bar=0.2 μm).

X–ray diffraction patterns for the precipitates of mullite–zirconia composites, which were calcined

at various temperatures, are shown in **Fig. 4.**
These data show that $Zr(OH)_4$ was amorphous
below 800°C and tetragonal ZrO_2 formed above
800°C in the composite. The formation of
mullite phase again occurred by an exothermic
reaction at 1250°C.

A TEM photograph of the mullite–ZrO_2 com-
posite powders calcined at 1300°C for 1 h is
shown in **Fig. 5.** It was found that dark par-
ticles were t–ZrO_2 particles surrounded by the
mullite agglomerates, which was confirmed by
electron diffraction pattern of the particles
shown in **Fig. 5(B).**

3—2. Microstructures of sintered bodies.

SEM microphotographs of etched surfaces of
pure mullite are shown in **Fig. 6.** In specimen
A, mainly acicular grains are seen, while in
specimens B and C microstructures are of
equiaxed grains, with α–Al_2O_3 particles dispers-
ed in the matrix of specimen C. The apparent-
ly unique microstructure observed in specimen
A may be explained in terms of the large
amount of the liquid phase formed during
sintering[13].

SEM and TEM photographs of the mullite–
ZrO_2 composites are shown in **Fig. 7.** Dense
mullite–ZrO_2 bodies, having ZrO_2 particles
dispersed uniformly in the matrices, were ob-
tained. As for the microstructure of mullite–
ZrO_2 composites, it was reported that ZrO_2 par-
ticles were either inter- or intragranular, depen-
ding on the fabrication methods[14]. ZrO_2 particles were mainly intragranular in the mullite–ZrO_2
composites fabricated by reaction sintering of Al_2O_3 and $ZrSiO_4$ powder mixtures, while they were in-
tergranular when the composites were formed using the mechanical mixture of fused mullite and
ZrO_2 powders. In the present studies using the co-precipitate as the starting powder, most of ZrO_2
particles were intergranular, but about 3% of ZrO_2 particles were intragranular as shown in **Fig.
7(C), (D), (E).**

On the other hand, an interesting phenomenon could be seen with regard to the grain morphology
of the mullite matrices. In **Fig. 7(C), (D), (E),** the microstructure of the mullite matrices were same
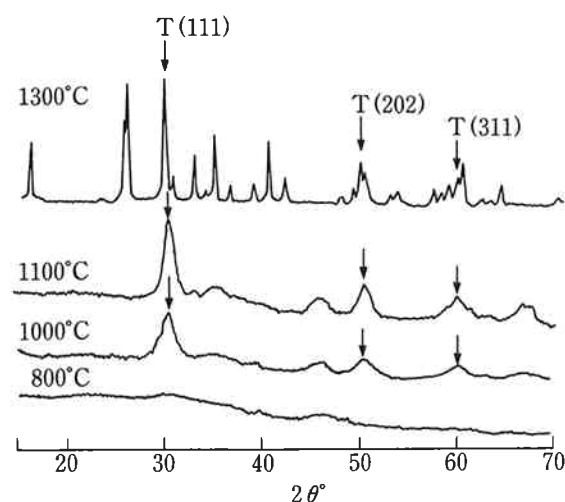as that of pure mullite.

3—3. Mechanical properties

Fig. 4. X-ray diffraction patterns for the
precipitates of mullite–zirconia com-
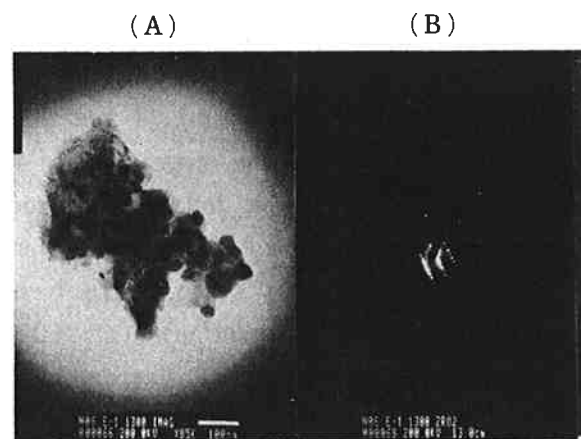posites, which were calcined at various
temperature.

(A)   (B)

Fig. 5. (A): A TEM photograph of the mullite–
ZrO_2 composite powder calcined at
1300°C for 1 h, (B): the electron diffrac-
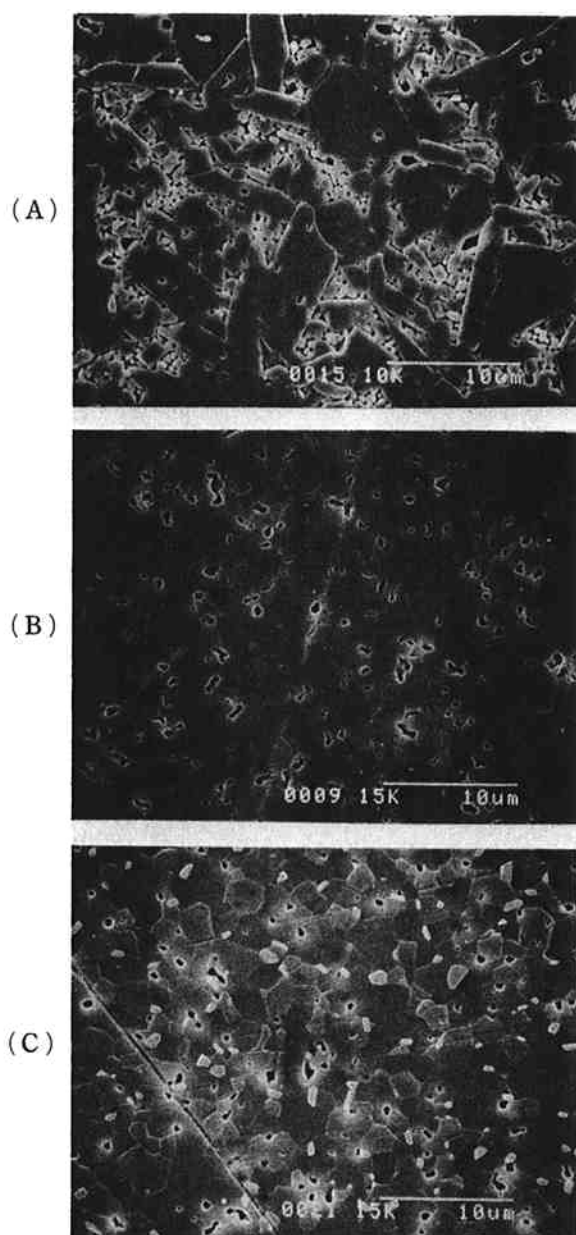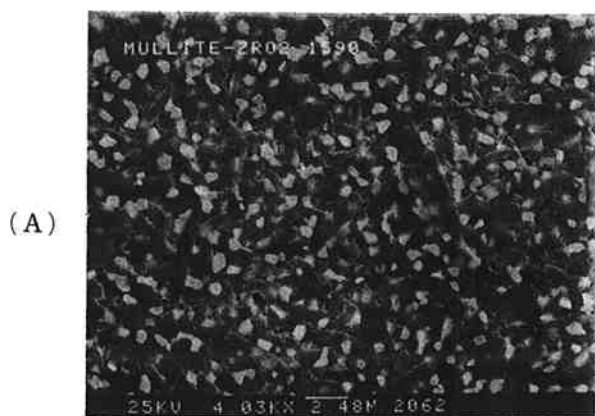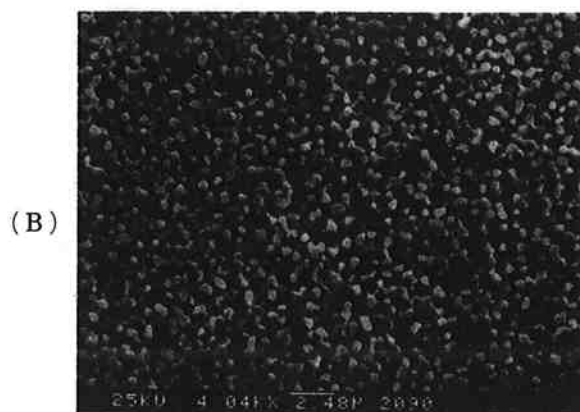tion pattern of the dark particle.

(A)

(B)

(C)

Fig. 6. SEM microphotographs of etched surface of
mullites and mulite-zirconia composites, (A),
(B), (C): sintered at 1650°C, 3 h.

(A)

Mullite (72)−10 vol % ZrO$_2$

(B)

Mullite (74)−20 vol % ZrO$_2$

(C) Mullite(72)-10vol%ZrO₂   500nm

(D) Mullite(74)-10vol%ZrO₂   500nm
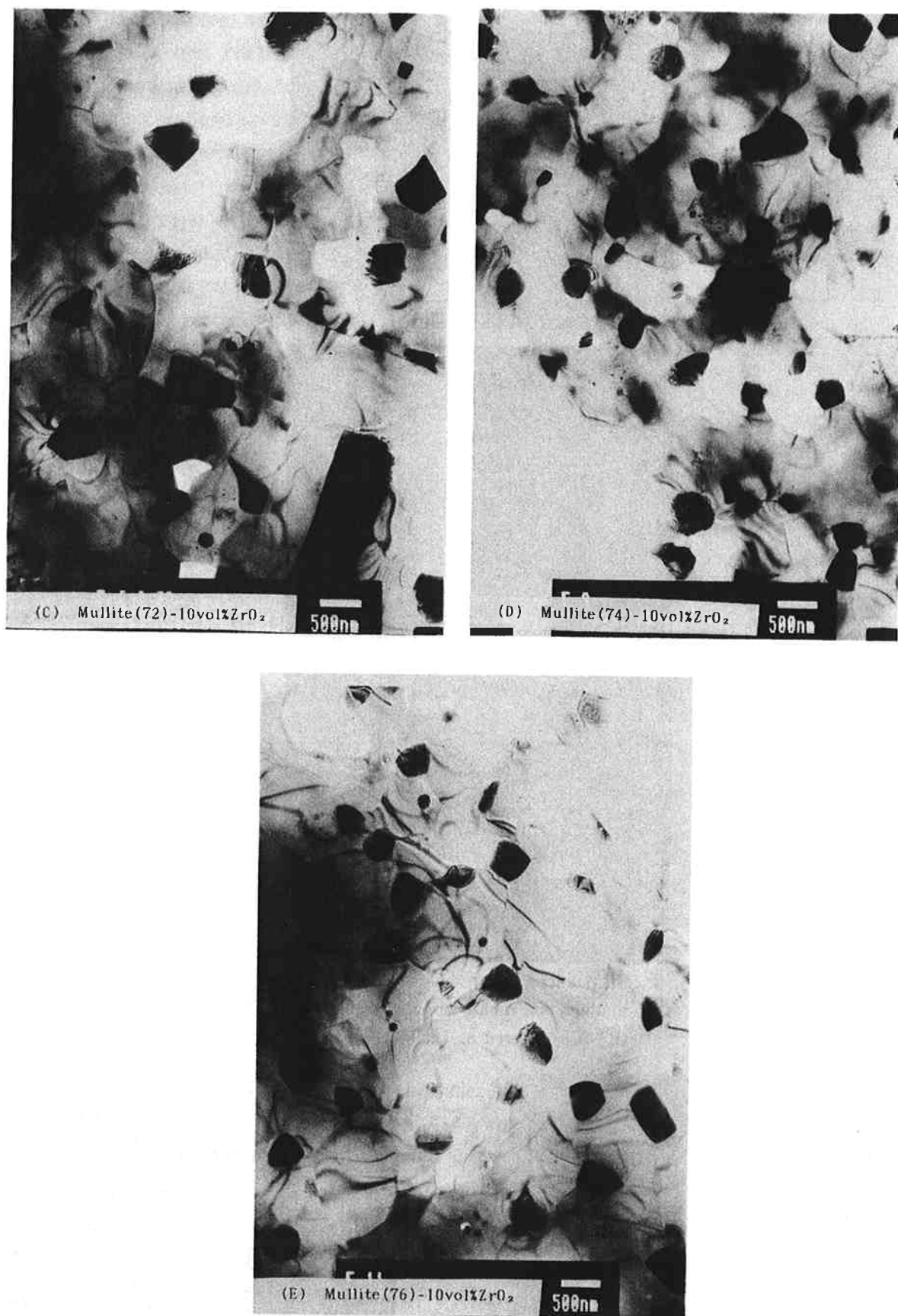
(E) Mullite(76)-10vol%ZrO₂   500nm

Fig. 7. SEM and TEM photographs of the mullite-ZrO₂ com-
posites, (A) (C) (D) and (E) sintered at 1620°C for 3 h,
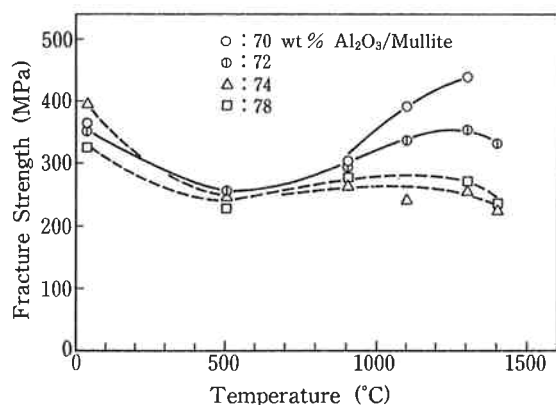(B) at 1590°C for 3 h.

Fig. 8. The temperature dependence of fracture strength obtained for the specimens with Al_2O_3 contents in the range of 70 to 78 wt%, all specimens were sintered at 1650°C, 3 h.
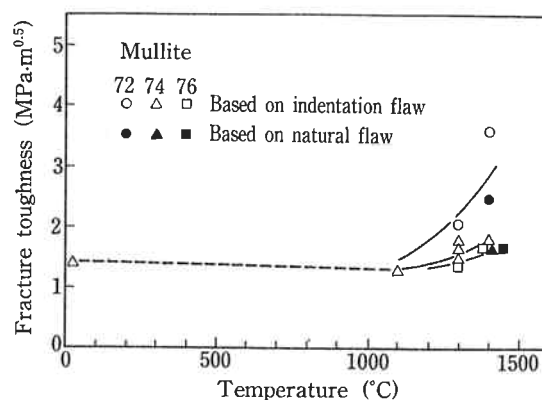
Fig. 9. Fracture toughness for specimens with 72, 74 and 76 wt% Al_2O_3 sintered at 1700°C plotted as a function of temperature.

3—3—1. Mullite

The results of bending strength between room temperature and 1400°C for four compositions of Al_2O_3/SiO_2 are shown in Fig. 8. From these results, it is found that the fracture strength is essentially independent of composition from room temperature to 900°C, with the minima in all the strength curves around 500°C. This figure also shows that in the temperature range of 900°C to 1300°C mullites with 70 and 72 wt% Al_2O_3 exhibit a significant increase in their fracture strength, while mullites with 74 and 78 wt% Al_2O_3 have little or no change. Fig. 9. shows K_{1c} for specimens with 72, 74 and 76 wt% Al_2O_3 at various temperatures. In this figure, the K_{1c} values obtained using the fracture-initiating flaw size, measured by SEM fractography are also shown as full symbols. Typical fracture topographies of the specimens precracked and tested at 1300°C and 1400°C are shown in Fig. 10. Although the fracture surface of a specimen tested at 1100°C did not reveal the presence of slow crack growth (SCG), in the specimen tested at 1300°C and 1400°C SCG this was observed. Completely intergranular fracture can be seen in the SCG region in the SEM microphotographs of Fig. 10. Mullites with 70 and 72 wt% Al_2O_3 were found to increases in both σ_f and K_{1c} above 1300°C, where SCG was observed. These increases in σ_f and K_{1c} were explained by the dominance of energy dissipation through plastic relaxation in the plastic zone over grain boundary sliding due to the presence of a glassy phase[15]. The appearance of SCG around 1300°C and above suggests the presence of an amorphous phase along the grain boundaries. It seems that the amount of the glassy phase at the grain boundary of mullite increases with decreasing Al_2O_3 content. The glassy phase seems to contribute to the fracture strength more in mullite with 70 and 72 wt% Al_2O_3 than those with 74 and 78 wt% Al_2O_3. The other contributing cause for the higher strength in mullite with 70 wt% Al_2O_3 is the non-equiaxed and grain structure which suppresses gross deformation and deflects crack propagation.

3—3—2. Mullite-zirconia composites

Fracture strength and toughness at room temperature as a function of ZrO_2 volume fraction of two different Al_2O_3 to SiO_2 ratio in mullite are shown in Fig. 11. The fracture strength and toughness
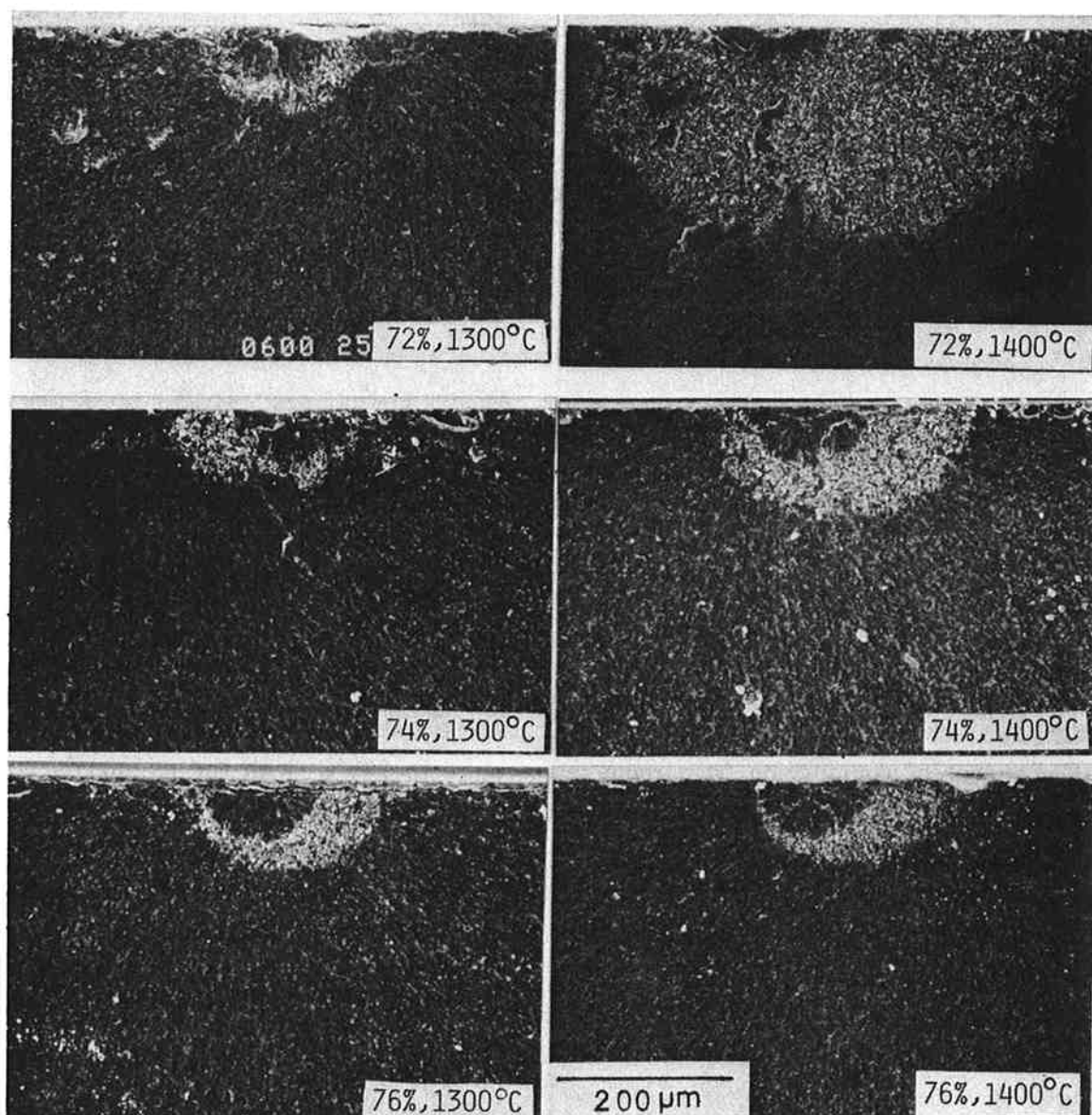
Fig. 10. Typical fracture topographies of the specimens precracked and tested at 1300°C and 1400°C.

increased with increasing total ZrO_2 volume fraction. As seen in **Fig. 12**, when the total ZrO_2 volume fraction in the mullite–ZrO_2 composites increased, the grain size of ZrO_2 increased, and the tetragonal fraction of ZrO_2 sharply decreased. As compared with the results of the composite fabricated by milling of fused mullite and ZrO_2 powder[16], the increase in ZrO_2 particle size was small, while the t–ZrO_2 fraction decreased significantly. The stability of t–ZrO_2 particles in ceramic matrices depends on the particle characteristics such as its size, shape, and distribution; furthermore, it seems to be influenced by the constrictive force acting on the ZrO_2 particles in the ZrO_2 toughened ceramics. Increasing the ZrO_2 fraction reduces the constrictive force exerted on ZrO_2. Furthermore, as shown in **Fig. 7**, most of the ZrO_2 particles were intergranular in the present mullite–ZrO_2 composites. Intergranular particles are less resistant to transformation, because they are less stable than intragranular particles[17]. In mullite–10 vol% ZrO_2 composite the fracture toughness increased with increasing t–ZrO_2 fraction as shown in **Fig. 13**. This fact indicats that
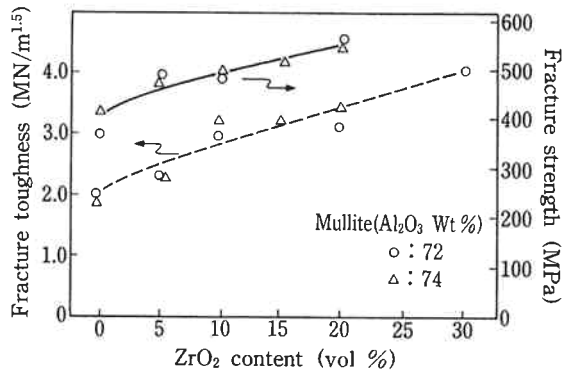
Fig. 11. Fracture strength and toughness at room temperature as a function of ZrO_2 volume fraction for two compositions of Al_2O_3/SiO_2, specimens (except the mullite-10 vol% ZrO_2 sintered at 1610°C for 3 h) were sintered at 1590°C for 3 h.
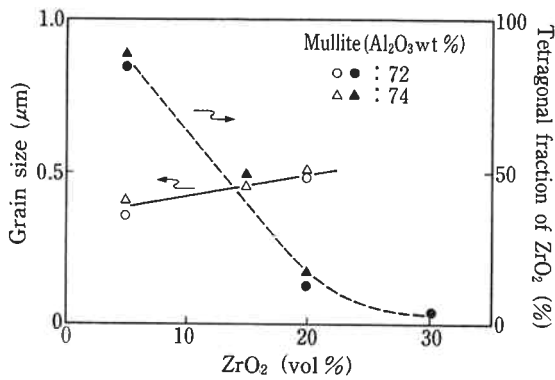

Fig. 12. ZrO_2 particle size and tetragonal fraction of ZrO_2 as a function of total ZrO_2 volume fraction, sintering conditions were the same as in Figure-3.

Fig. 13. The fracture toughness as a function of tetragonal ZrO_2 fraction in the mullite-10 vol% ZrO_2 composites, the fraction of t-ZrO_2 were controlled by sintering at different temperatures.

Fig. 14. The temperature dependence of the fracture strength of the composites mullite (72)+ZrO_2(5 and 20 vol%) sintered at 1590°C for 3 h.

the transformation toughening is one of the toughening mechanisms as reported by Wallace [14]. On the other hand, the extrapolated fracture toughness value at $ZrO_2=0$ does not coincide with the measured value of pure mullite, which indicats that other toughening mechanisms such as micro-cracking[18] and crack deflection[19] are activated in the present composites.

The temperature dependence of the fracture strength of the composites mullite(72)+ZrO_2(5 and 20 vol%) and mullite(74)+ZrO_2(5, 15 and 20 vol%) are shown in Fig. 14 and15. The fracture strength of all specimens was higher than that of pure mullite. The fracture strength decreased monotonically with increasing temperatures up to 900°C, and approached the same value of mullite (72 and 74) with no ZrO_2 additions at 900°C. In the temperature range of 900°C to 1300°C, the
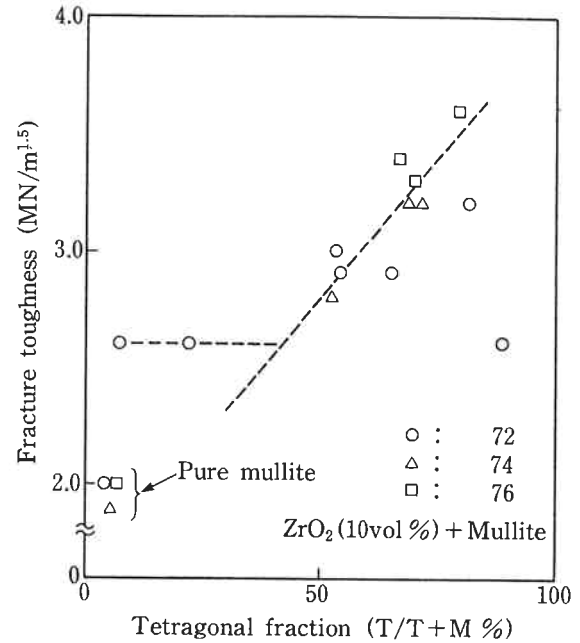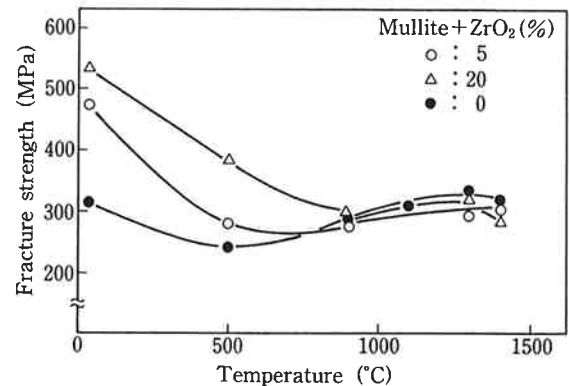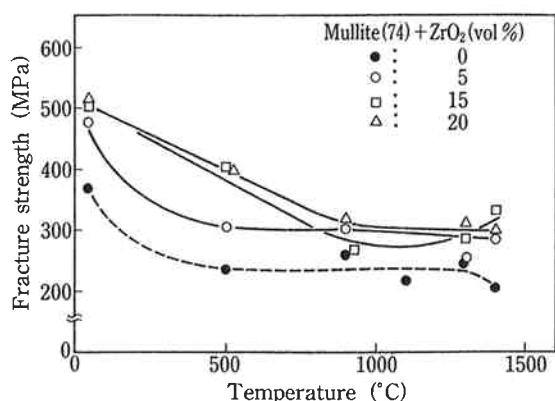
Fig. 15. The temperature dependence of the fracture strength of the composites mullite(74)+ZrO₂(5, 15 and 20 vol%) sintered at 1590°C for 3 h.

temperature dependence of the strength of the composites seems to be generally similar to that of pure mullite without effects of t-ZrO₂ on fracture strength by toughening and of little contribution of both micro-cracking and crack deflection.

4. Conclusion

1) The products precipitated from aqueous solution of Al(NO₃)₃ mixed with colloidal SiO₂ transform to mullite with an exotherm reaction at 1250°C.

2) In the range of 70 to 78 wt% Al₂O₃, the composition 70 wt% Al₂O₃ shows the highest fracture strength above 1000°C because of a glassy phase present along the grain boundaries and the acicular grain shape.

3) Dense mullite–ZrO₂ composites, having ZrO₂ particles dispersed uniformly in the matrices, were obtained form a co-precipitation method. Most of ZrO₂ particles were intergranular. Furthermore, the microstructural features of the mullite matrices depend on the Al₂O₃/SiO₂ ratios of the mullite.

4) Fracture strength of mullite–ZrO₂ composites increased with increasing total ZrO₂ volume fraction in a temperature range from room temperature to 900°C. The toughening mechanism seems to be a combination of transformation toughening and other mechanisms such as microcracking and/or crack deflection.

References

1) H. Yamad and S. Kimura; *J. Ceram. Assoc. Japan,* **70**, 65, 1962.

2) K. S. Mazdiyasni and L. M. Brown; *J. Am. Ceram. Soc.,* **55**, 548, 1972.

3) T. A. Wheat, E. M. H. Sallam and A. C. D. Chaklader; *Ceramurgia Int.,* 2, 42, 1979.

4) N. Claussen and J. Jahn; *J. Am. Ceram. Soc.,* **63**, 228, 1980.

5) G. Orange et al.; *J. Mater. Sci.,* **20**, 2533, 1985.

6) J. S. Moya and M. I. Osendi; *J. Mater. Sci.,* **19**, 2909, 1984.

7) J. J. Petrovic and M. G. Mendiratta; "Fracture Mechanics Applied to Brittle Materials, ASTM. STP 678", Edited by S. W. Freiman, ASTM, pp. 83-102.

8) R. C. Garvie and P. S. Nicholson; *J. Am. Ceram. Soc.,* **55**, 303, 1972.

9) K. Nihara, R. Morena and D. P. Hasselman; *J. Mater. Sci.,* **1**, 13, 1982.

10) D. W. Hoffman, R. Roy and S. Komarneni; *J. Am. Ceram. Soc.,* **67**, 468, 1984.

11) A. K. Chakraborty and D. K. Ghosh; *J. Am. Ceram. Soc.,* **61**, 170, 1978.

12) S. Kanzaki, H. Tabata and T. Kumazawa; *J. Am. Ceram. Soc.,* **68**, c-6, 1985.

13) S. Prochazka and F. J. Klug; *J. Am. Ceram. Soc.,* **66**, 874, 1983.

14) J. S. Wallace, N. Claussen and S. Prochazka; *Proc. of International Synposium on Ceramic components for Engine,* 1983 Japan.

15) TAI-IL MAH and K. S. Mazdiyasni; *J. Am. Ceram. Soc.,* **66**, 700, 1983.

16) S. Prochazka, J. S. Wallace and N. Claussen; *J. Am. Ceram. Soc.,* **66**, c–125, 1983.

17) A. H. Heuer, N, Claussen, W. M. Kriven and M. Rühle; *J. Am. Ceram. Soc.,* **65**, 642, 1982.

18) N. Claussen, R. C. Cox and J. S. Wallace; *J. Am. Ceram. Soc.,* **65**, c–190, 1982.

19) K. Faber and A. G. Evans; *Acta Metall.,* **31**, 565, 1983.